Integrative Omics Reveals Subtle Molecular Perturbations Following Ischemic Conditioning in a Porcine Kidney Transplant Model

Darragh P. O'Brien[1*], Adam M. Thorne[1,2*], Honglei Huang[1,2], Elisa Pappalardo[3], Xuan Yao[1], Peter Søndergaard Thyrrestrup[4,5], Kristian Ravlo[4,6], Niels Secher[6,7], Rikke Norregaard[4,6], Rutger J. Ploeg[2], Bente Jespersen[4,6], Benedikt M. Kessler[1]

[1]Target Discovery Institute, Centre for Medicines Discovery, Nuffield Department of Medicine, University of Oxford, UK

[2]Nuffield Department of Surgical Sciences and Oxford Biomedical Research Centre, University of Oxford, UK

[3]Sir William Dunn School of Pathology, University of Oxford, UK

[4]Department of Renal Medicine, Aarhus University Hospital, Aarhus, Denmark

[5]Department of Anaesthesiology, Aalborg University Hospital, Aalborg, Denmark

[6]Department of Clinical Medicine, Aarhus University, Aarhus, Denmark

[7]Department of Anaesthesiology and Intensive Care Medicine, Aarhus University Hospital, Aarhus Denmark

*These authors contributed equally

Corresponding authors:

darragh.obrien@ndm.ox.ac.uk; rutger.ploeg@nds.ox.ac.uk; bente.jespersen@clin.au.dk; benedikt.kessler@ndm.ox.ac.uk

Running Title:

Integrative Omic Profiling of a Porcine Kidney Transplant Model

ABSTRACT

Background: Remote Ischemic Conditioning (RIC) has been proposed as a therapeutic intervention to circumvent the ischemia/reperfusion injury (IRI) that is inherent to organ transplantation. Using a porcine kidney transplant model, we aimed to decipher the subclinical molecular effects of a RIC regime, compared to non-RIC controls.

Methods: Kidney pairs (n = 8+8) were extracted from brain dead donor pigs and transplanted in juvenile recipient pigs following a period of cold ischemia. One of the two kidney recipients in each pair was subjected to RIC prior to kidney graft reperfusion, while the other served as non-RIC control. We designed a modern integrative Omics strategy combining transcriptomics, proteomics, and phosphoproteomics to deduce molecular signatures in kidney tissue that could be attributed to RIC.

Results: In kidney grafts taken out 10 h after transplantation we detected minimal molecular perturbations following RIC compared to non-RIC at the transcriptome level, which was mirrored at the proteome level. In particular, we noted that RIC resulted in suppression of tissue inflammatory profiles. Furthermore, an accumulation of muscle extracellular matrix assembly proteins in kidney tissues was detected at the protein level, which may be in response to muscle tissue damage and/or fibrosis. However, the majority of these protein changes did not reach significance ($p<0.05$).

Conclusions: Our data identifies subtle molecular phenotypes in porcine kidneys following RIC and this knowledge could potentially aid optimization of remote ischemic conditioning protocols in renal transplantation.

Key Words:

Remote Ischemic Conditioning, Kidney Transplantation, Proteomics, Transcriptomics, Integrative Omics, Inflammation

BACKGROUND

Organ donation and transplantation inevitably involve periods of both warm and cold ischemia, due to diminished or restricted blood flow, which deprives the donor organ tissue of the oxygen required to maintain cellular metabolism. Subsequent reperfusion at time of implantation of the ischemic graft results in tissue damage including several molecular hallmarks, such as hypoxic stress and production of reactive oxygen species, a rapid reduction of ATP levels, intracellular acidosis, and diminished nutritional supplies [1]. Combined, these insults lead to the activation of apoptotic and necrotic pathways, and if uncorrected, to organ dysfunction, rejection, and eventually graft fibrosis [2]. Acute kidney injury (AKI) induced by ischemia and subsequent reperfusion is called delayed graft function in the clinical transplant setting and leads to the need of dialysis as well as a risk of poorer transplant outcome [3]. Remote ischemic conditioning (RIC) has been proposed as a therapeutic modality to mitigate the effects of ischemia/reperfusion injury (IRI) in organ transplantation [4, 5]. RIC is a simple procedure which creates short and repetitive cycles of non-damaging ischemia, usually applied to a leg or arm, which may reduce damaging effects caused by IRI in the target organ. RIC has shown various outcomes in pre-clinical studies in both kidney and other organs such as lung, liver, small intestine and in a variety of situations and species [6-12]. Several pre-clinical studies have demonstrated a reduction in IRI and improved early graft function in the recipient [13-16]. Regarding kidney transplantation and AKI, a protective effect of RIC in rodent renal models has been described, however the transition into the human setting has been challenging [15, 17]. Our previous work in a porcine model of kidney transplantation suggested a beneficial effect of RIC on early graft perfusion and function evidenced by a significantly improved renal plasma perfusion and glomerular filtration rate (GFR) [18]. However, when RIC was applied to kidney transplant patients in a clinical trial

70 (CONTEXT), no clinical benefit was observed, although the trial did reveal distinct subclinical effects
71 on kidney transplants at the molecular level [17, 19, 20]. We have therefore revisited our RIC study
72 carried out in pigs that had shown potential positive effects of RIC which stimulated us to design the
73 clinical CONTEXT study. Using samples obtained from our original porcine RIC model [18], we have
74 now studied whether we could detect any proteomic and transcriptomic changes in recipient tissue
75 using advanced quantitative mass spectrometry and RNA sequencing. In this study, we describe
76 changes in molecular profiles comparable to the ones observed in human kidneys subjected to RIC.

77

78 **METHODS**

79 **Transplant model**

80 The effects of RIC versus non-RIC controls in porcine kidney transplants were evaluated in a paired
81 randomized study, the design of which was described in detail by Soendergaard et al [18]. Briefly,
82 eight kidney pairs were taken from eight brain-dead donor pigs (60-64 kg) and transplanted into
83 sixteen bilateral nephrectomized recipient pigs (14–16 kg), which were randomly given RIC or non-
84 RIC within each pair. Prior to organ reperfusion, RIC was performed as indicated below. Pigs were
85 surveyed, under anesthesia, for 10 h after transplantation, assessing renal function by GFR, renal
86 plasma perfusion and known renal biomarkers. The study was approved by the National Committee
87 on Animal Research Ethics no. 2008-561-1584 (Animal Experiments Inspectorate, Copenhagen,
88 Denmark) and conducted in accordance with the "Principles of Laboratory Animal Care" (NIH
89 publication Vol. 25, No. 28 revised 1996).

90 **Sample retrieval and ischemia regimen**

91 Kidney retrieval, transplantation and RIC was performed by experienced transplant surgeons as
92 described previously (**Figure 1**) [18]. Briefly, female Danish Landrace pigs were anaesthetized and
93 placed under mechanical ventilation. Ringer's acetate was infused to maintain fluid balance and

94 arterial pressure. Brain death was induced by increasing intracranial pressure. Kidneys were
95 extracted, perfused and stored in 5°C cold storage solution. Two recipients were transplanted
96 simultaneously after having their native kidneys removed. A RIC regimen was undertaken whereby
97 the abdominal aorta was clamped above the aortic bifurcation but below the renal arteries in four
98 cycles, with each cycle consisting of 5 min of ischemia and 5 min of reperfusion. Surgeons and
99 investigators were unblinded to the treatment during the experiments. Renal biopsies from kidneys
100 in the RIC and non-RIC groups were taken prior to termination after 10 hours reperfusion and snap
101 frozen in liquid nitrogen for transcriptomic and proteomic analysis.

102 **Transcriptomics analysis**

103 ***Sample preparation.*** Sixteen tissue samples from the kidney medulla and cortex (weighing
104 approximately 20 mg) were lysed using a Precellys 24 homogenizer (Bertin Instruments) in 350 µL of
105 RNeasy Mini kit RLT lysis buffer. RNA was then extracted using RNeasy Mini kit (Qiagen, cat number:
106 74104) as per manufacturer's instructions. Purified RNA was eluted in 40 µL RNase-free H_2O and the
107 approximate concentration evaluated using a NanoDrop ND-1000 spectrophotometer.
108 Approximately, 450 ng of purified RNA was converted to cDNA by using high-capacity reverse
109 transcription kit (Applied Biosystems, cat number: 4368814). For each reaction, a mix of 2 µL 10x RT
110 buffer, 0.8 µL 25x dNPT mix, 2 µL 10x RT random primers, 1 µL Multiscribe reverse transcriptase, 3.2
111 µL nuclease free H_2O and 11 µL of RNA (40.9 ng/µL) was prepared. This was then primed at 25°C for
112 10 min, incubated at 37°C for 120 min and inactivated at 85°C for 5 min in a thermal cycler (VWR
113 UNO 96). cDNA was then stored at -20°C until further use. Transcriptomics analysis was performed
114 on ~50 fmol of the sample library and sequenced on a NextSeq 500 sequencer (Illumina) achieving,
115 ~30 million reads in total **(Supplementary Table 1)**. An overview of the transcriptomics workflow is
116 given in **Figure 1**.

117 For transcriptomics data analysis, FASTQ files were converted to Binary-sequence Alignment Format
118 (BAM) files using HISAT2 (v2.1.0) and Samtools (v1.3). The DESeq2 R package (Bioconductor) was
119 used for normalization, visualization, and differential analysis of the data. Furthermore, BAM files

120 were also imported into Perseus software (v1.6.0.2) for comparative analysis, and genome
121 annotation was performed using the *Sus scrofa* FASTA cDNA database (http://www.ensembl.org).
122 Reads per kilo per million (RPKM) values were calculated by a normalization step dividing by the sum
123 (Normalization→Divide), followed by dividing normalized values by gene length, multiplying by 109,
124 and taking the $\log_2$ values. The transcriptomics dataset was deposited in ArrayExpress (AE) at EBI
125 under the accession number E-MTAB-10872 [21].

126 ***q-PCR.*** For q-PCR, primers for selected genes of interest were designed using Primer BLAST (see
127 Table 1 for sequences), parameters included spanning exon-exon junctions, a target size of 200 bp
128 and a maximum product size of 150. A Beta-Actin control gene was used as a reference [22]. A total
129 of 20 µg of cDNA was used for each 20 µL reaction, in combination with 200 nM of each forward and
130 reverse primer (Invitrogen) and Fast SYBR Green Master Mix (Applied Biosystems, cat number:
131 4385612), according to the manufacturer's instructions. The reaction plates were run on a Roche
132 Lightcycler 480, with an initial pre-incubation of 37°C for 30 sec, then denaturing at 95°C for 3 sec,
133 followed by annealing at 60°C for 30 sec. Denaturing and annealing was repeated for 40 runs before
134 conducting melt curve analysis. Using Roche Lightcycler analysis software, the noise band was
135 altered to exclude any background noise whilst staying within the lower third of the linear section of
136 the curve to gain initial Ct values. Average Ct values for Beta-Actin were then subtracted from
137 average Ct values of target genes to get dCt. RIC vs non-RIC groups and different time points were
138 then compared using 2^-(x-y) to obtain relative expression levels and plotted on a box-dot graph.

139 **Proteomics analysis**

140 ***Sample preparation.*** In accordance with the transcriptomics study, sixteen tissue samples (weighing
141 approximately 20 mg) were lysed using a Precellys 24 homogenizer (Bertin Instruments) in 30 µL
142 RIPA and 6M urea lysis buffer per 1 mg of tissue. Samples were reduced with 200 mM tris(2-
143 carboxyethyl)phosphine (TCEP) at 55°C for 1 hour and alkylated with 375 mM iodoacetamide (IAA)
144 for 30 min at room temperature. Following this, protein precipitation via methanol/chloroform
145 precipitation was performed. The resulting pellet was dried and resuspended in 50 µL

146 triethylammonium bicarbonate (TEAB) and the protein concentration determined using a BCA assay
147 (Pierce). In total, 100 µg of protein was digested by trypsin using the SMART method (Thermo
148 Scientific). In brief, each sample was loaded into a SMART digestion tube (Thermo Fisher Scientific,
149 Cat no 60109-103) containing 150 µL of SMART digestion buffer. These were then incubated at 70°C
150 at 1400 rpm for 2 hours on a heat shaker (Eppendorf) and spun at 2500 x g for 5 min, with collection
151 of the supernatant. Samples were de-salted using SOLAµ SPE plates (Thermo Scientific, Cat no
152 60109-103). Columns were equilibrated using 100% acetonitrile (ACN), then 0.1% trifluoroacetic acid
153 (TFA). The samples were then diluted with 1% TFA and pulled through the column using a vacuum
154 pump. They were then washed with 0.01% TFA and eluted in 100 µL 65% acetonitrile. Eluates were
155 dried using a vacuum concentrator (SpeedVac, Thermo Scientific) and resuspended in 100 µL of 100
156 mM TEAB for Tandem Mass Tag (TMT) labelling.

157 ***TMT labelling and high pH fractionation.*** TMT 10plex reaction groups were used to label the
158 digested peptides. Groups comprised of 8 samples (4 sets of RIC and non-RIC) and two pools; one
159 undiluted, and one diluted 1:5, with the pools allowing us to assess the dynamic range of the
160 measurement. For labelling, 41 µL of TMT label was added to each sample and incubated for 1 hour
161 at room temperature. To quench the reaction, 8 µL of 5% hydroxylamine was added to each sample
162 and incubated at room temperature for 15 minutes. Equal volumes of each RIC and non-RIC sample
163 were then pooled into their respective groups to generate a RIC and non-RIC "pooled" sample, and
164 de-salted using Sep-Pak C18 columns. The resulting eluent was dried using a vacuum concentrator
165 (SpeedVac, Thermo Scientific) and resuspended in 120 µL of buffer A (98% MilliQ-H2O, 2%
166 acetonitrile, 0.1% TFA). The two combined TMT 10plex experiments were then pre-fractionated
167 using high pH 10.0 reversed-phase liquid chromatography (HPLC) into a total of 100 fractions.
168 Fractions were subsequently concatenated into a total of 20 samples and submitted for LC-MS/MS
169 analysis. The proteomic sample preparation strategy is summarized in **Figure 1**.

170 ***Phosphoproteomics.*** For phosphopeptide enrichment, 50 µg of protein was removed from each of
171 the 16 tissue samples and pooled into their respective RIC and non-RIC groups. Samples were
172 reduced, alkylated, digested with trypsin, and desalted as above. Peptides (~400 µg) were eluted
173 from Sep-Pak cartridges in 500 µL buffer B (65% ACN, 35% MilliQ-H2O, and 0.1% TFA).
174 Phosphopeptide enrichment was performed using an Immobilized Metal Affinity Chromatography
175 (IMAC) column with the aid of a Bravo Automated Liquid Handling Platform (Agilent) according to
176 manufacturer's instructions.

177 ***Mass Spectrometry analysis.*** Liquid chromatography tandem mass spectrometry (LC–MS/MS)
178 analysis was undertaken using a Dionex Ultimate 3000 nano-ultra reversed-phase HPLC system with
179 on-line coupling to a Q Exactive High Field (HF) mass spectrometer (Thermo Scientific). Samples were
180 separated on an EASY-Spray PepMap RSLC C18 column (500 mm × 75 µm, 2 µm particle size;
181 Thermo Fisher Scientific) over a 60 min gradient of 2–35% ACN in 5% dimethyl sulfoxide (DMSO),
182 0.1% FA, and the flow rate was ~ 250 nL/min. The mass spectrometer was operated in data-
183 dependent analysis mode for automated switching between MS and MS/MS acquisition. Full MS
184 survey scans were acquired from 400–2000 *m/z* at a resolution of 60,000 at 200 *m/z* and the top 12
185 most abundant precursor ions were selected for high collision energy dissociation fragmentation.
186 MS2 fragment ion resolution was set to 15,000.

187 ***Data analysis.*** MS raw data files were searched using Proteome Discoverer (v2.3; total proteome)
188 and MaxQuant (v1.5.14; phosphoproteome) software packages. Search parameters included the
189 allowance of two missed trypsin cleavages. Carbamidomethylation (C) was set as a fixed
190 modification, while TMT6plex (N-term, K), oxidation (M), deamidation (N, Q), and phosphorylation
191 (STY) were set as variable modifications where appropriate. The data was searched against porcine
192 protein sequences using the *UPR_Sus scrofa* fasta file (as of August 2019), along with the
193 corresponding decoy reverse database. Only unique and razor peptides were used for quantitation.

194 **Statistical analysis.** TMT 10plex quantitation and data analysis was performed in Perseus software
195 (v1.6.0.2) which filtered out contaminant and false positive identifications (decoys). The data were
196 $\log_2$ transformed, and replicates were grouped into RIC and non-RIC. Missing values were imputed
197 from the normal distribution and all samples were normalized by median subtraction. Hierarchical
198 cluster analysis was performed on all the proteins identified by LC–MS/MS and visualized as heat
199 maps using the Pearson correlation algorithm. Volcano plots were generated by applying parametric
200 Student's t-tests between RIC and non-RIC controls. A Christmas tree plot was generated for the
201 phosphoproteomics data where only one replicate was acquired. The mass spectrometry proteomics
202 data have been deposited to the ProteomeXchange Consortium via the PRIDE [23] partner
203 repository with the dataset identifier PXD025273. Gene Ontology and biological pathway
204 enrichment analysis was performed using STRING protein–protein interaction networks & functional
205 enrichment analysis (https://string-db.org/).

206

207 **RESULTS and DISCUSSION**

208 We first performed RNA sequencing on renal cortex and medulla tissues of kidney grafts to quantify
209 changes at the transcriptome level (**Figure 1**). A total of 19,220 transcripts were successfully
210 quantified across RIC and non-RIC groups (**Supplementary Tables 1 and 2**). In total, 33 transcripts
211 had at least a two-fold change in abundance between groups, at a *p*-value of ≤ 0.05 (**Figure 2,**
212 **Supplementary Table 3**). The most notable of these included heat shock protein beta-1 (HSPB1),
213 monocarboxylate transporter 4 (SLC16A3), C-X-C motif chemokine (CXCL13), C-C motif chemokine 2
214 (CCL2), interleukin-1 receptor type 2 (IL1R2), interleukin-1 beta (IL1B), leukotriene B4 receptor 1
215 (LTB4R), Na(+)/H(+) exchange regulatory cofactor NHE-RF4 (PDZD3), and Ras-like protein family
216 member 10A (RASL10A), all of which were significantly down-regulated following RIC. Moreover,
217 biological pathway analysis revealed a reduction in the transcripts of genes associated with
218 regulation of inflammation following RIC as compared to their non-RIC counterparts (**Figure 2,**

219 **Supplementary Figure 1**). Transcript changes were confirmed by performing qPCR on a selected
220 panel of targets which were observed to be dysregulated in RIC in either our dataset, or as
221 previously described in literature. We measured five genes in total in a pooled sample of each group,
222 including IL1B, LTB4R, PDZD3, SLC16A3, and RASL10A (**Supplementary Table 4**). We observed a slight
223 increase in RIC induced SLC16A3 transcripts, but overall, none of the genes quantified reached
224 statistically significance between RIC and non-RIC, with all having a *p*-value of > 0.2 (**Figure 3**).

225 Following the analysis of the kidney donor biopsies at the transcriptome level, we extended the
226 study to measure changes between the kidney tissue proteomes of the respective RIC and non-RIC
227 groups. Our quantitative proteomic strategy (**Figure 1**) successfully quantified a total of 7,546
228 proteins across all samples (**Supplementary Table 5**). Hierarchical clustering analysis revealed no
229 clear discrimination between RIC and non-RIC groups at the proteome level (**Figure 2A**). Similarly,
230 and in agreement with the transcriptomics results, the majority of proteins were found to be
231 unchanged between groups. To determine if we could identify trends in the data, we took those
232 proteins with the largest ($\geq \log_2 0.5$), albeit non-significant, fold changes forward for further analysis.
233 In this context, 252 proteins were deemed to be differentially expressed between RIC and non-RIC
234 groups (**Supplementary Table 6**). Mirroring the transcriptomics results, a dampening of immune
235 response proteins was observed in RIC versus non-RIC tissue, whereby the largest fold changes were
236 observed in approximately 15 Ig-like domain-containing proteins (**highlighted in green in Figure 2B**).
237 Attenuation of proteins involved in the inflammatory response associated with IRI could be one of
238 the primary beneficial factors that could contribute to RIC renoprotection. This dampening may
239 serve as a natural defense mechanism against the destruction caused by IRI. Despite this, the
240 inflammatory response generally associated with renal transplantation, in the form of apoptotic cell
241 death, macrophage and neutrophil infiltration, and anti-inflammatory cytokine production, was
242 found to be unaffected by RIC in the pigs studied [24]. We performed pathway enrichment analysis
243 on the differentially expressed proteins. Unfortunately, the Ig-like species described above could not
244 be included due to lacking a mature porcine gene entry (**Supplementary Figure 2**). Mirroring the

245 human CONTEXT study [19], there was an accumulation of muscle-derived and extracellular matrix
246 assembly proteins in the renal tissue following RIC, including the collagens COL1A2, COL2A1,
247 COL4A2, COL4A, COL6A3, fibrillin and fibulin (**Figure 2, Supplementary Figure 2**), although no
248 tourniquet on a limb but rather clamping of the aorta was used in the present porcine study.
249 Additionally, upregulation of factors associated with innate immunity such as lysosome-associated
250 membrane glycoprotein 1 (LAMP1), neutrophil cytosol factor 2 (NCF2), leucine-rich alpha-2-
251 glycoprotein (LRG1), myeloperoxidase (MPO), and properdin (CFP) were observed, suggesting the
252 technique provoked the activation of tissue remodeling cascades within the organ itself.
253 Upregulation of these factors provide a favorable environment for wound-healing and repair, and
254 collagen scaffolds have been shown to enhance survival of transplanted cardiomyoblasts and
255 improve function in ischemic rat hearts [25]. Increased collagen production has also been associated
256 with a response to the hypoxic or anoxic conditions inherent to surgery, ultimately leading to
257 adhesion development [26]. It is, however, unclear if these proteins provide a protective mechanism
258 in RIC, or just the consequence of tissue damage which could lead to fibrosis. Furthermore, we
259 identified an up-regulation of several components of the blood coagulation cascade, including
260 Vitamin K-dependent protein C (PROC), Fibrinogen beta chain (FGB), and Plasminogen (PLG).
261 Interestingly, SLC16A3, IL1B, LTB4R, RASL10A, and CXCL13, which were found to have some of the
262 largest changes at the transcript level, were not detected at the proteome level, while HSPB1,
263 LTB4R, and PDZD3 transcripts were differentially abundant, but found to be unchanged between
264 non-RIC and RIC groups at the protein level.

265 To gain more insight into the signaling dynamics underlying these molecular changes in kidney
266 tissue, we performed phosphoproteomics to compare a global pool of all 8 RIC samples to that of
267 the 8 non-RIC controls. We identified 3,524 phosphosites across both groups, from a total of 3,626
268 proteins (**Supplementary Table 7**). No substantial differences were identified in the
269 phosphoproteome between RIC and non-RIC groups, indicating little steady-state effects of RIC on
270 kidney tissue at the indicated time point (**Supplementary Figure 3**).

271 To determine if a joint analysis could reveal useful insights that could not be deciphered from
272 individual analysis alone, we integrated the transcriptomic and proteomic datasets (**Figure 4A**). Once
273 again, the Ig-like proteins that were found to be down-regulated in RIC in the proteomics dataset
274 alone (**Figure 2B**) could not be included in this type of analysis due to a lack of matching cognate
275 sequences at the transcriptome level. A low correlation was observed between the two datasets,
276 with a Pearson correlation coefficient of 0.017. We subsequently performed 2D Annotation
277 Enrichment Analysis in an effort to identify pathways which were simultaneously up- or down-
278 regulated in both datasets [27]. Up-regulated biochemical pathways in RIC versus non-RIC and
279 common to both datasets included muscle tissue development/remodeling, extracellular matrix
280 disassembly, ubiquitin-specific protease activity, and steroid hormone receptor activity (**Figure 4**).
281 Conversely, down-regulated pathways in RIC versus non-RIC and common to both included kidney
282 development, vasodilation, epidermal growth factor receptor signaling and the regulation of
283 myoblast differentiation.

284 A possible explanation for the absence of substantial and significant proteomic and transcriptomic
285 changes may be attributed to the condition of kidney tissue used in this study. The tissue had been
286 exposed to multiple insults, including brain death, periods of cold and warm ischemia and
287 reperfusion. This makes it increasingly difficult to fully dissect the (perhaps comparatively minor)
288 effects of RIC, despite a more aggressive RIC regimen than that used in the human setting. A limiting
289 factor of this study concerning -Omics profiling is the number of available samples, and the
290 timepoint at which the analyzed biopsies were taken after a 10-hour observation phase. This may be
291 too early of a time point to measure a significant change in protein expression, which is possibly
292 reflected in the lack of change identified at the proteomic depth achieved in this study, although the
293 transcriptome profile would not support this notion. Ideally, there would be an observation phase of
294 several days with multiple biopsies. Finally, with the disappointing clinical effects of RIC, the positive
295 effects of RIC regarding GFR and graft reperfusion in the related pig study could reflect a type 1 error
296 or generally reflect a subtle phenomenon observed in this animal model [18].

CONCLUSIONS

In summary, RIC of the pig recipient before kidney graft transplantation with reperfusion, similar to what was observed in human counterparts, did not result in substantial molecular changes/perturbations in the graft compared to non-RIC controls. The data did suggest, however, that the administered RIC caused a potentially detrimental accumulation of muscle proteins in the kidney graft tissue, and also triggered a subtle interplay between the innate and adaptive immune response, with a dampening of the latter. Ultimately, however, our discovery studies showed no major differences in the transcriptomes and proteomes of porcine kidney transplant tissue following RIC, despite excellent depth of coverage in each. Our results, therefore, support the conclusion that the RIC protocol used does not substantially protect against ischemia/reperfusion injury.

LIST OF ABBREVIATIONS

AKI – Acute Kidney Injury

ATP – adenosine triphosphate

GFR – Glomerular Filtration Rate

IRI – Ischemic/Reperfusion Injury

RIC – Remote Ischemic Preconditioning

TMT – Tandem Mass Tag

DECLARATIONS

ETHICS APPROVAL AND CONSENT TO PARTICIPATE

Kidney graft tissue samples were taken from the porcine RIC study [18].

CONSENT FOR PUBLICATION

All authors have read the manuscript and given their consent for publication.

AVAILABILITY OF DATA AND MATERIALS

The mass spectrometry raw data files have been deposited under PRIDE Submission PXD025273. The transcriptomics dataset was deposited in ArrayExpress (AE) at EBI under the accession number E-MTAB-10872.

COMPETING INTERESTS

The authors have no conflicts of interest to declare

FUNDING

Funding was provided by the Novo Nordisk Foundation, The Danish Medical Research Council, The Danish Kidney Association (Nyreforeningen), Department of Clinical Medicine, Aarhus University, Nuffield Department of Medicine, University of Oxford, and Nuffield Department of Surgical Sciences, University of Oxford.

AUTHORS CONTRIBUTIONS

DOB, AT, HH, EP, XY, PS, KR and NS performed the experiments. BJ, RJP and BMK conceptualized the study. DOB, AT, BJ, RJP and BMK wrote the manuscript. DOB, AT, HH, EP, PS, KR and NS analyzed the data. All authors read and approved the final manuscript.

ACKNOWLEDGEMENTS

The authors would like to thank members of the Kessler, Jespersen, and Ploeg research groups for helpful discussions and technical support.

AUTHORS' INFORMATION

341 Darragh P O'Brien and Adam M Thorne contributed equally to the work

342

343 ***Affiliations***

344 **Target Discovery Institute, Centre for Medicines Discovery, Nuffield Department of Medicine,**
345 **University of Oxford, UK**

346 Darragh P O'Brien, Adam M Thorne, Honglei Huang, Xuan Yao, Benedikt M Kessler

347 **Nuffield Department of Surgical Sciences and Oxford Biomedical Research Centre, University**
348 **of Oxford, UK**

349 Adam M Thorne, Honglei Huang, Rutger J Ploeg

350 **Sir William Dunn School of Pathology, University of Oxford, UK**

351 Elisa Pappalardo

352 **Department of Renal Medicine, Aarhus University Hospital, Aarhus, Denmark**

353 Bente Jespersen, Peter Søndergaard Thyrrestrup, Kristian Ravlo

354 **Department of Anaesthesiology, Aalborg University Hospital, Aalborg, Denmark**

355 Peter Søndergaard Thyrrestrup

356 **Department of Clinical Medicine, Aarhus University, Aarhus, Denmark**

357 Rikke Norregaard, Bente Jespersen, Kristian Ravlo and Niels Secher

358 **Department of Anesthesiology and Intensive Care Medicine, Aarhus University Hospital, Aarhus**
359 **Denmark**

360 Niels Secher

361

362

363 **FIGURE LEGENDS**

364 **Figure 1.** ***Overview of transcriptomic and proteomic workflows***. **A**) For transcriptomics, tissue
365 samples were cut, weight and lysed. RNA was extracted, followed by cDNA library preparation, and
366 the difference in transcript level determined between non-RIC and RIC groups. For selected targets
367 of interest, qPCR was undertaken. **B**) In the proteomics arm, proteins were extracted, reduced,
368 alkylated and subjected to methanol/chloroform extraction, digested with trypsin, cleaned-up and
369 subjected to 10plex TMT labelling. Labelled peptides were separated by high pH-RP, prior to analysis
370 by LC-MS/MS. The green boxes outline our sample pooling and fractionation strategy. A total of 16
371 tissue samples (and 4 pools) were labelled across two TMT kits, with 8 RIC and non-RIC pairs and 2
372 pools per 10plex kit. Each TMT experiment was subsequently separated into 100 fractions, which
373 were then concatenated down into 20 fractions. This resulted in a final total of 40 samples for
374 injection into the mass spectrometer.

375 **Figure 2.** ***Transcriptome and proteome changes by RIC*** **A**) The top left-hand corner displays Box
376 plots of $\log_2$ normalized data. The heat map displays the regularized log-transformed data for the
377 top differentially expressed transcripts. The PCA plot visualizes the regularized log-transformed data
378 which minimizes differences between samples for rows with small counts, and which normalizes
379 with respect to library size. Finally, the MA plot shows the $\log_2$ fold changes attributable to a given
380 variable over the mean of normalized counts. Red points have adjusted p-value less than 0.05. **B**)
381 Volcano plot displaying differential transcriptome expression. The x-axis measures expression
382 difference by $\log_2$(fold change), and the y-axis indicates statistical significance by $-\log_{10}$(*p*-value).
383 Down-regulated species are coloured blue, while their up-regulated counterparts are coloured red.
384 Enriched biological processes (Gene Ontology) determined from differentially regulated transcripts
385 (displayed by their gene symbol) are listed underneath the plot. **C)** Hierarchical clustering analysis of
386 RIC and non-RIC proteomes. **D)** Volcano plot displaying differential proteome expression. Down-
387 regulated immunoglobulins of interest are circled in green.

388 **Figure 3.** ***Minimal transcriptional alteration by RIC***. No statistically significant difference was
389 observed for any of the selected qPCR targets (IL1B, LTB4R, PDZD3, SLC16A3, and RASL10A) between
390 RIC and non-RIC groups, with all *p*-values > 0.2.

391 **Figure 4.** ***Integrated Omics reveals RIC induced tissue leakage and reduced inflammation***. A)
392 Scatter plot of the *Log_2-fold-change* between RIC and non-RIC groups of the proteomics on the x-
393 axis, versus the transcriptomics on the y-axis. Species which are down-regulated in both datasets are
394 coloured blue, while their up-regulated counterparts are coloured red. A low Pearson correlation
395 coefficient of 0.017 was observed. B) 2D Annotation Enrichment Analysis generated using transcripts
396 and proteins which were commonly dysregulated across the two datasets.

397

398 **Supplementary Figure S1.** ***Transcriptomic pathway enrichment analysis reveals subtle alteration of***
399 ***tissue inflammation by RIC***. All transcripts (n=33) which were found to be dysregulated in RIC versus
400 non-RIC controls were searched against the *Sus scrofa* database in STRING. Only interactions of the
401 highest confidence (scores > 0.90) were included in the analysis. Genes associated with immune
402 regulation are highlighted, with those linked to interleukin biology coloured red, while cytokines are
403 coloured purple.

404 **Supplementary Figure S2.** ***Proteomic pathway enrichment analysis uncovers RIC induced tissue***
405 ***leakage and altered inflammation***. Proteins (n=252) which were found to have the greatest
406 dysregulation in RIC versus non-RIC controls were searched against the *Sus scrofa* database in
407 STRING. Only interactions of the highest confidence (scores > 0.90) were included in the analysis.
408 Proteins/genes of interest are highlighted, with proteins associated with muscle and ECM coloured
409 in blue, blood coagulation in green, and factors associated with innate immunity coloured red.

410 **Supplementary Figure S3.** ***Kidney tissue phosphoproteomics unaffected by RIC***. A) Abundance plots
411 indicate no significant difference in the phosphoproteome between RIC and control groups. B) A

412 Christmas tree plot, with Significance B thresholds colour coded. Minor changes were observed
413 between groups.

414

415 **Table 1:** ***List of gene names and primer sequences used to conduct qPCR.*** A total of five genes were
416 selected for qPCR validation of transcriptomics results, with beta actin serving as a control.

417 **Supplementary Table 1:** ***Transcriptome sequence alignments.*** An average sequence alignment of
418 82% was achieved across all samples

419 **Supplementary Table 2:** ***List of transcripts identified by transcriptomics.*** A total of 19,220
420 transcripts were successfully identified across groups.

421 **Supplementary Table 3:** ***Transcripts differentially expressed between RIC and Non-RIC groups.***

422 **Supplementary Table 4:** ***qPCR validation on a panel of targets from discovery transcriptomics.*** IL1B,
423 LTB4R, PDZD3, SLC16A3, and RASL10A were quantified by qPCR. We observed a slight increase in RIC
424 induced SLC16A3 transcripts, but overall, none of the genes quantified reached statistically
425 significance between RIC and non-RIC, with all having a *p*-value of > 0.2

426 **Supplementary Table 5:** ***List of proteins identified by proteomics.*** A total of 7,546 proteins were
427 successfully identified across groups.

428 **Supplementary Table 6:** ***Proteins differentially expressed between RIC and Non-RIC groups.***

429 **Supplementary Table 7:** ***List of proteins and phosphosites identified by phosphoproteomics.*** A total
430 of 3,524 phosphosites were successfully identified across groups.

431

432

433

434 **TABLES**

Oligo Name	Forward Sequence (5' - 3')	Reverse Sequence (5' - 3')	Scale (µmole)
PDZD3	CCCTGTAAGTGCCCTGCTAT	CTCCAGGGATCAGAAGGATCG	0.025µmole
LTB4R	TGGTACTTCCTCTCTGGCTGA	CCATTGCAAGGACAGGCTTT	0.025µmole
RASL10A	TTGCATTTGGGGTAAACCTGGAA	GCCACTCCTCCAAGCTTAATTC	0.025µmole
SLC16A3	AGGTAACCTGAGACCTGGCT	TGGTTCCGCGTCCCTGG	0.025µmole
IL1B	CCAATTCAGGGACCCTACCC	GTTTTGGGTGCAGCACTTCAT	0.025µmole
Beta Actin	TGTCATGGACTCTGGGGATG	GGGCAGCTCGTAGCTCTTCT	0.025µmole

435

436 **Table 1: List of gene names and primer sequences used to conduct qPCR.** A total of five genes were
437 selected for qPCR validation of transcriptomics results, with beta actin serving as a control.

438

439

440

441 **REFERENCES**

442 1. Wu, M.Y., et al., *Current Mechanistic Concepts in Ischemia and Reperfusion Injury.* Cell
443 Physiol Biochem, 2018. **46**(4): p. 1650-1667.
444 2. Zhao, H., et al., *Ischemia-Reperfusion Injury Reduces Long Term Renal Graft Survival:*
445 *Mechanism and Beyond.* EBioMedicine, 2018. **28**: p. 31-42.
446 3. Sharfuddin, A.A. and B.A. Molitoris, *Pathophysiology of ischemic acute kidney injury.* Nat Rev
447 Nephrol, 2011. **7**(4): p. 189-200.
448 4. Zhou, D., et al., *Remote ischemic conditioning: a promising therapeutic intervention for*
449 *multi-organ protection.* Aging, 2018. **10**(8): p. 1825-1855.
450 5. Thuret, R., et al., *Ischemic pre- and post-conditioning: current clinical applications.* Prog Urol,
451 2014. **24 Suppl 1**: p. S56-61.
452 6. Jiang, T., et al., *The Role of Remote Ischemic Preconditioning in Ischemia-Reperfusion Injury*
453 *in Rabbits with Transplanted Lung.* Clin Lab, 2015. **61**(5-6): p. 481-6.
454 7. Vasdekis, S.N., et al., *The role of remote ischemic preconditioning in the treatment of*
455 *atherosclerotic diseases.* Brain Behav, 2013. **3**(6): p. 606-16.
456 8. Vrakas, G., et al., *Synergistic Effect of Ischemic Preconditioning and Antithrombin in*
457 *Ischemia-Reperfusion Injury.* Exp Clin Transplant, 2017. **15**(3): p. 320-328.
458 9. Magyar, Z., et al., *Beneficial effects of remote organ ischemic preconditioning on micro-*
459 *rheological parameters during liver ischemia-reperfusion in the rat.* Clin Hemorheol
460 Microcirc, 2018. **70**(2): p. 181-190.
461 10. Saeki, I., et al., *Ischemic preconditioning and remote ischemic preconditioning have*
462 *protective effect against cold ischemia-reperfusion injury of rat small intestine.* Pediatr Surg
463 Int, 2011. **27**(8): p. 857-62.
464 11. Qi, B., et al., *Effect of remote ischemic preconditioning among donors and recipients*
465 *following pediatric liver transplantation: A randomized clinical trial.* World J Gastroenterol,
466 2021. **27**(4): p. 345-357.

467 12. Roubille, F., et al., *Effects of remote ischemic conditioning on kidney injury in at-risk patients*
468 *undergoing elective coronary angiography (PREPARE study): a multicenter, randomized*
469 *clinical trial.* Sci Rep, 2019. **9**(1): p. 11985.
470 13. Wu, G., et al., *Effect of remote ischemic preconditioning on hepatic ischemia-reperfusion*
471 *injury in patients undergoing liver resection: a randomized controlled trial.* Minerva
472 Anestesiol, 2020. **86**(3): p. 252-260.
473 14. Tuncer, F.B., et al., *Ischemic Preconditioning and Iloprost Reduces Ischemia-Reperfusion*
474 *Injury in Jejunal Flaps: An Animal Model.* Plast Reconstr Surg, 2019. **144**(1): p. 124-133.
475 15. Jung, K.W., et al., *Effect of Remote Ischemic Preconditioning Conducted in Living Liver Donors*
476 *on Postoperative Liver Function in Donors and Recipients Following Liver Transplantation: A*
477 *Randomized Clinical Trial.* Ann Surg, 2020. **271**(4): p. 646-653.
478 16. Fuller, T.F., et al., *Ischemic preconditioning improves rat kidney graft function after severe*
479 *ischemia/reperfusion injury.* Transplant Proc, 2005. **37**(1): p. 377-8.
480 17. Krogstrup, N.V., et al., *Remote Ischemic Conditioning on Recipients of Deceased Renal*
481 *Transplants Does Not Improve Early Graft Function: A Multicenter Randomized, Controlled*
482 *Clinical Trial.* Am J Transplant, 2017. **17**(4): p. 1042-1049.
483 18. Soendergaard, P., et al., *Improved GFR and renal plasma perfusion following remote*
484 *ischaemic conditioning in a porcine kidney transplantation model.* Transpl Int, 2012. **25**(9): p.
485 1002-12.
486 19. Thorne, A.M., et al., *Subclinical effects of remote ischaemic conditioning in human kidney*
487 *transplants revealed by quantitative proteomics.* Clin Proteomics, 2020. **17**(1): p. 39.
488 20. Nielsen, M.B., et al., *Remote ischaemic conditioning and early changes in plasma creatinine*
489 *as markers of one year kidney graft function-A follow-up of the CONTEXT study.* PLoS One,
490 2019. **14**(12): p. e0226882.
491 21. Athar, A., et al., *ArrayExpress update - from bulk to single-cell expression data.* Nucleic Acids
492 Res, 2019. **47**(D1): p. D711-d715.
493 22. Li, Q., et al., *Evaluation of potential reference genes for relative quantification by RT-qPCR in*
494 *different porcine tissues derived from feeding studies.* Int J Mol Sci, 2011. **12**(3): p. 1727-34.
495 23. Perez-Riverol, Y., et al., *The PRIDE database and related tools and resources in 2019:*
496 *improving support for quantification data.* Nucleic Acids Res, 2019. **47**(D1): p. D442-d450.
497 24. Secher, N., et al., *No effect of remote ischaemic conditioning on inflammation in a porcine*
498 *kidney transplantation model.* Transpl Immunol, 2014. **31**(2): p. 98-104.
499 25. Kutschka, I., et al., *Collagen matrices enhance survival of transplanted cardiomyoblasts and*
500 *contribute to functional improvement of ischemic rat hearts.* Circulation, 2006. **114**(1 Suppl):
501 p. I167-73.
502 26. Saed, G.M. and M.P. Diamond, *Hypoxia-induced irreversible up-regulation of type I collagen*
503 *and transforming growth factor-beta1 in human peritoneal fibroblasts.* Fertil Steril, 2002.
504 **78**(1): p. 144-7.
505 27. Cox, J. and M. Mann, *1D and 2D annotation enrichment: a statistical method integrating*
506 *quantitative proteomics with complementary high-throughput data.* BMC Bioinformatics,
507 2012. **13 Suppl 16**(Suppl 16): p. S12.

508

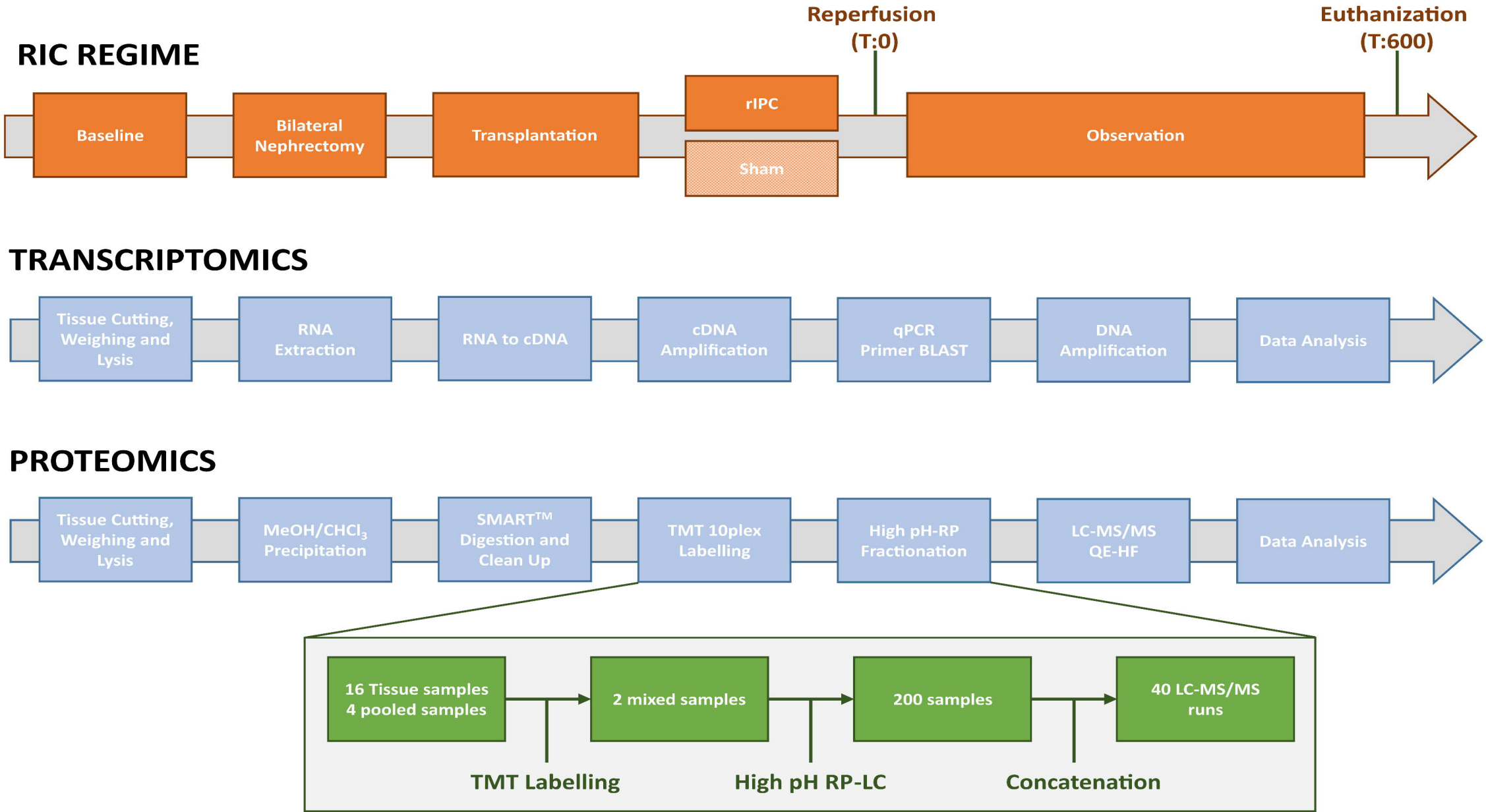
RIC REGIME
Reperfusion (T:0)
Euthanization (T:600)
Baseline
Bilateral Nephrectomy
Transplantation
rIPC
Sham
Observation
TRANSCRIPTOMICS
Tissue Cutting, Weighing and Lysis
RNA Extraction
RNA to cDNA
cDNA Amplification
qPCR Primer BLAST
DNA Amplification
Data Analysis
PROTEOMICS
Tissue Cutting, Weighing and Lysis
MeOH/CHCl3 Precipitation
SMART™ Digestion and Clean Up
TMT 10plex Labelling
High pH-RP Fractionation
LC-MS/MS QE-HF
Data Analysis
16 Tissue samples 4 pooled samples
2 mixed samples
200 samples
40 LC-MS/MS runs
TMT Labelling
High pH RP-LC
Concatenation

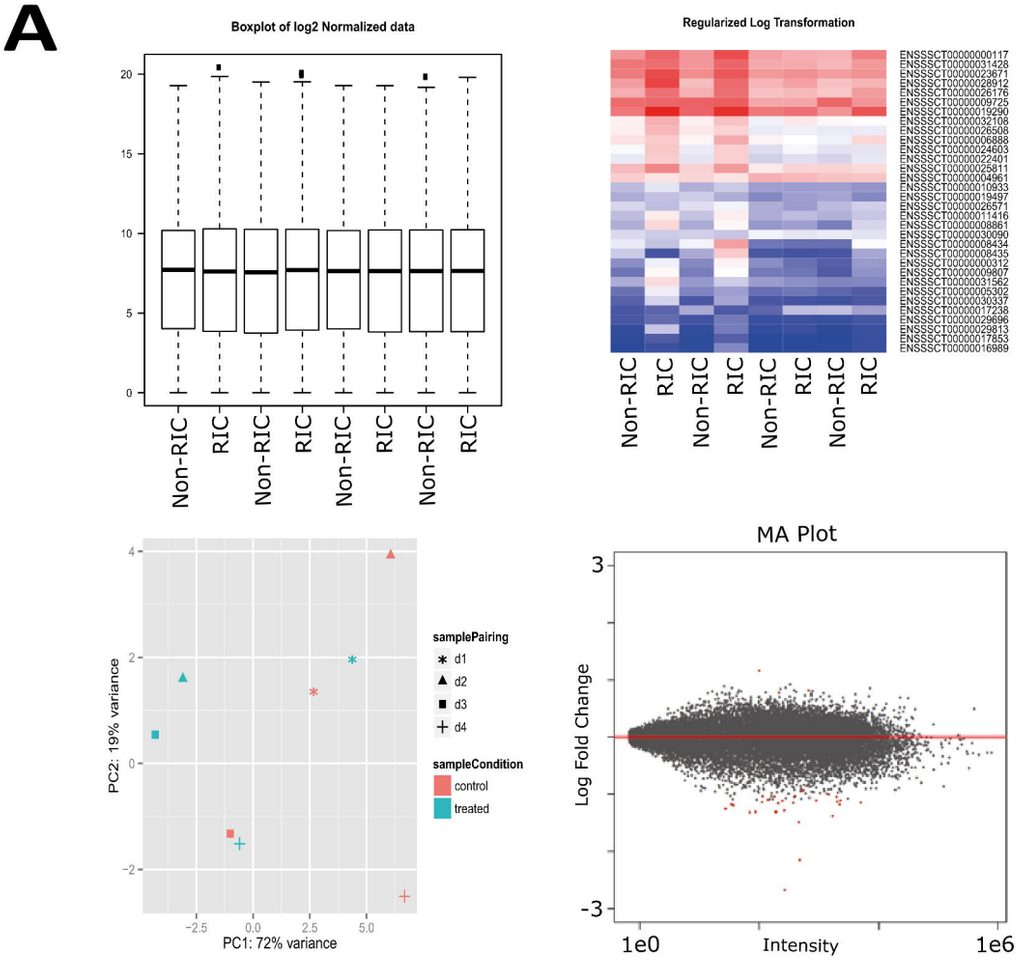

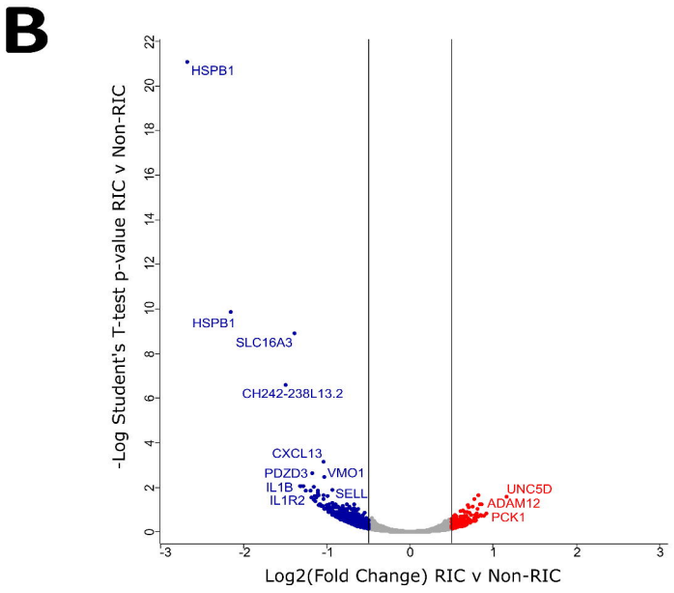

	Biological Process (Gene Ontology)			
GO-term	*Description*	*Count in Network*	*Strength*	*False Discovery*
GO:0044344	cellular response to fibroblast growth factor stimulus	2 of 6	2.46	0.0142
GO:0071347	cellular response to interleukin-1	2 of 10	2.24	0.0142
GO:0030593	neutrophil chemotaxis	2 of 10	2.24	0.0142
GO:0002688	regulation of leukocyte chemotaxis	2 of 12	2.16	0.0142
GO:0070098	chemokine-mediated signalling pathway	2 of 13	2.12	0.0142
GO:0071222	cellular response to lipopolysaccharide	2 of 17	2.01	0.0142
GO:0071356	cellular response to tumor necrosis factor	2 of 20	1.94	0.0142
GO:0045786	negative regulation of cell cycle	2 of 29	1.78	0.0142
GO:0019221	cytokine-mediated signalling pathway	3 of 56	1.67	0.0142
GO:0006954	inflammatory response	3 of 62	1.62	0.0142
GO:0006928	movement of cell or subcellular component	3 of 66	1.59	0.0142
GO:0022603	regulation of anatomical structure morphogenesis	2 of 49	1.55	0.0142
GO:0015031	protein transpot	2 of 53	1.51	0.0142
GO:0051050	positive regulation otransport	2 of 59	1.47	0.0147
GO:0016192	vesicle-mediated transport	2of 64	1.43	0.0154
GO:0002682	regulation of immune system process	3 of 103	1.40	0.0142

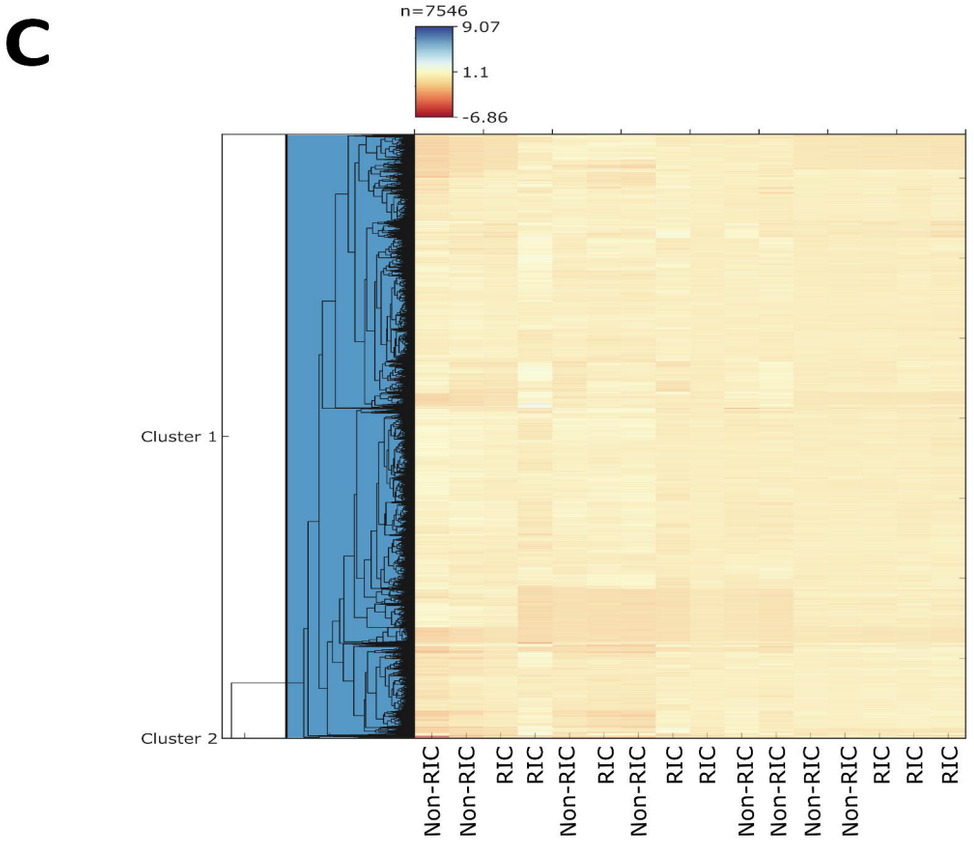

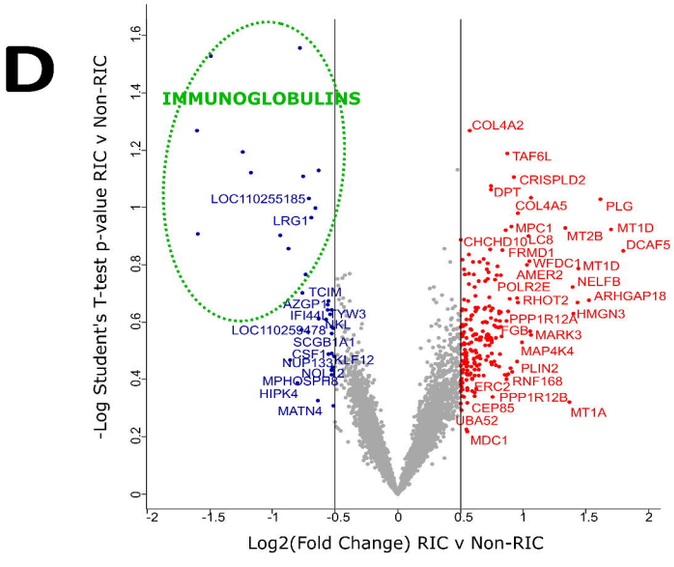

	Biological Process (Gene Ontology)			
Pathway	*Description*	*Count in Network*	*Strength*	*False Discovery*
SSC-419037	NCAM1 interactions	3 of 15	1.34	0.0244
SSC-1442490	Collagen degradation	4 of 38	1.06	0.0244
SSC-3000178	ECM Proteoglycans	4 of 40	1.04	0.0244
SSC-1650814	Collagen biosynthesis and modifying enzymes	5 of 55	1.00	0.0212
SSC-216083	Integrin cell surface interactions	5 of 64	0.93	0.0244
SSC-2022090	Assembly of collagen fibrils and other multimeric structures	4 of 53	0.92	0.0376
SSC-2565942	Regulation of PLK1 activity of G2/M Transition	5 of 69	0.90	0.0244
SSC-4420097	VEGFA-VEGFR2 pathway	5 of 74	0.87	0.0244
SSC-195258	RHO GTPase effectors	11 of 213	0.75	0.0014
SSC-69275	G2/M transition	7 of 146	0.72	0.0244
SSC-194315	Signaling by Rho GTPases	14 of 331	0.67	0.0014
SSC-9006934	Signalling by receptor tyrosine kinases	11 of 339	0.55	0.0244
SSC-2262752	Cellular responses to stress	9 of 279	0.55	0.0289
SSC-6798695	Neutrophil degranulation	12 of 382	0.54	0.0212
SSC-168249	Innate Immune System	18 of 707	0.45	0.0148
SSC-168256	Immune System	24 of 1240	0.33	0.0244

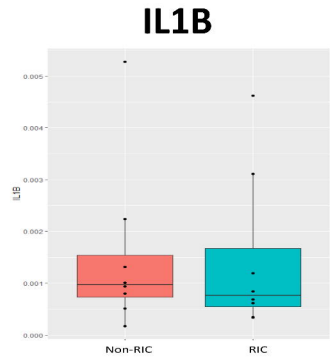

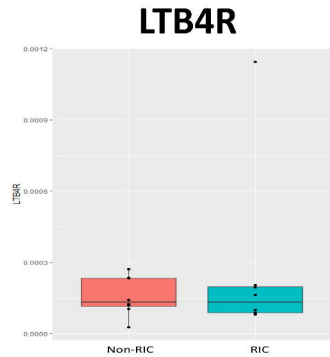

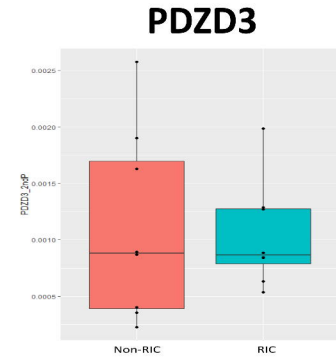

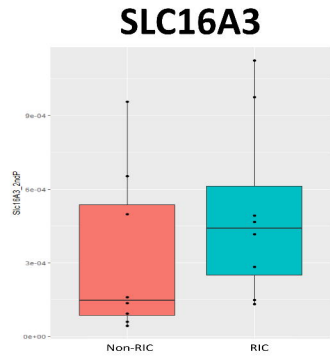

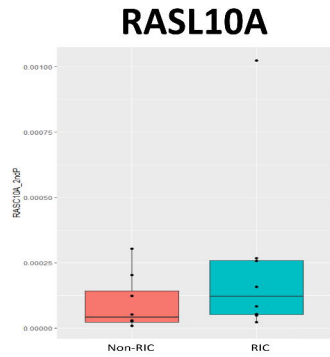

Gene	*p*-value (RIC v Non-RIC)
IL1B	0.942122575
LTB4R	0.414858107
PDZD3	0.842717016
SLC16A3	0.207829143
RASL10A	0.284549205

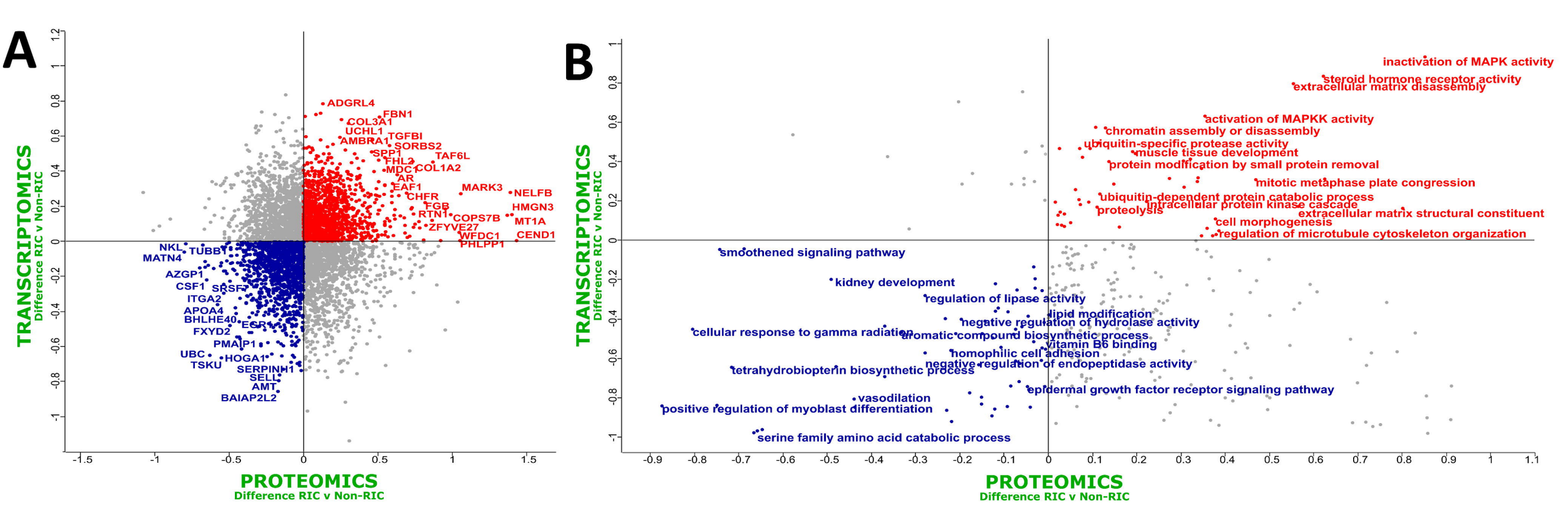
A
TRANSCRIPTOMICS
Difference RIC v Non-RIC
PROTEOMICS
Difference RIC v Non-RIC
ADGRL4
FBN1
COL3A1
UCHL1
TGFBI
AMBRA1
SORBS2
SPP1
TAF6L
FHL2
MDC1
COL1A2
AR
EAF1
MARK3
NELFB
CHFR
HMGN3
FGB
RTN1
COPS7B
MT1A
ZFYVE27
WFDC1
CEND1
PHLPP1
NKL
TUBB1
MATN4
AZGP1
CSF1
SRSF7
ITGA2
APOA4
BHLHE40
ECR1
FXYD2
PMAIP1
UBC
HOGA1
TSKU
SERPINH1
SELL
AMT
BAIAP2L2
B
TRANSCRIPTOMICS
Difference RIC v Non-RIC
PROTEOMICS
Difference RIC v Non-RIC
inactivation of MAPK activity
steroid hormone receptor activity
extracellular matrix disassembly
activation of MAPKK activity
chromatin assembly or disassembly
ubiquitin-specific protease activity
muscle tissue development
protein modification by small protein removal
mitotic metaphase plate congression
ubiquitin-dependent protein catabolic process
intracellular protein kinase cascade
proteolysis
extracellular matrix structural constituent
cell morphogenesis
regulation of microtubule cytoskeleton organization
smoothened signaling pathway
kidney development
regulation of lipase activity
lipid modification
negative regulation of hydrolase activity
cellular response to gamma radiation
aromatic compound biosynthetic process
vitamin B6 binding
homophilic cell adhesion
negative regulation of endopeptidase activity
tetrahydrobiopterin biosynthetic process
epidermal growth factor receptor signaling pathway
vasodilation
positive regulation of myoblast differentiation
serine family amino acid catabolic process